Available online at www.sciencedirect.com
SCIENCE DIRECT®
ELSEVIER
International Journal of Solids and Structures 42 (2005) 5831–5847
INTERNATIONAL JOURNAL OF SOLIDS and STRUCTURES
www.elsevier.com/locate/ijsolstr

Micromechanical analysis of failure in thin protective coatings

Asher A. Rubinstein *, Yaliang Tang

Department of Mechanical Engineering, Tulane University, 430 L. Boggs Building, New Orleans, LA 70118, USA

Received 20 October 2004
Available online 21 April 2005

Abstract

The integrity of protective coatings is the subject of this investigation. Specifically, we concentrate on the case of thermo-protective coatings, so-called thermal barrier coatings, aiming at development of methodology for service life estimation of the coated components under thermal loading. At the current phase of the development, we establish relationships between various thermal loading patterns and failure driving parameters at different failure stages by developing an analytical–computational model of the process. The analysis addresses a typical failure development pattern consisting of a system of multiple surface cracks leading to and branching along or near the interface between the coating and the base material. The process is driven by thermal stresses. The developed model is applicable to thin coatings and provides insight into the processes taking place during failure development and the effect of the details of the applied thermal loading.

The methods developed in the course of this investigation may be applied to the analysis of environmental effects on protective coatings and to investigations of failure development in layered composite systems under general loading conditions.
© 2005 Elsevier Ltd. All rights reserved.

Keywords: Protective coatings; Failure; Micromechanics; Fracture; Interface cracks

1. Introduction

The efficiency of aircraft engines can be improved significantly by increasing the temperature in the combustion chambers and the gas path temperatures in the high-pressure turbine sections. The temperatures in these areas of today's high thrust engines exceed the temperature capability of typical turbine metallic alloys. To combat this situation, thermal barrier coatings (TBCs) have been developed for application to

* Corresponding author. Tel./fax: +1 5048655771.
E-mail address: asher@tulane.edu (A.A. Rubinstein).

0020-7683/$ - see front matter © 2005 Elsevier Ltd. All rights reserved.
doi:10.1016/j.ijsolstr.2005.03.024

turbine and diesel engine components. A ceramic layer is deposited on a metallic alloy substrate. This combination gives the turbine components, such as turbine blades, for example, the benefits of the high temperature resistance of ceramics and the structural reliability of the metallic alloy.

TBCs are processed either by air plasma spray (APS) or electron beam vapor deposition (EB-PVD). The conditions of the working environment are extreme. The thermal cycle generates very high stresses due to extreme differences in the thermo-mechanical properties of the thermal barrier and the substrate. Eventually, critical failure of TBCs develops near or along the interface. There are numerous reports on experimental studies of the TBCs' behavior under various thermal loading conditions, which include failure development observation. For example, a comprehensive description of these process under different conditions and extensive reference lists are given by Zhu and Miller (1997, 1998a,b,c), and in some cases correlations of the experiment and FEM simulations are presented by Zhu et al. (1998). The operational conditions and the process of failure development in TBCs are complex. The developed computational models typically address isolated issues and are based on simplified physical systems. This is a natural trend due to the complexity of the systems and the nature of the problem. Several basic model developments have led to greater understanding of some aspects of crack growth within the TBCs or along the interface, and determined their quantitative characteristics. These must be noted; in particular, the key development work done by Rizk and Erdogan (1989), Hutchinson and Suo (1992), Hutchinson and Lu (1995), Lee and Erdogan (1998), Shulze and Erdogan (1998), Qian et al. (1998), Evans et al. (2001), Hsueh (2002).

In the current state of understanding of the process, the critical issue is the interfacial or near interfacial cracking in the TBCs. In practical terms, one needs to determine the actual fracture mechanics parameters that initiate internal microcracks and promote their growth during specific thermo-mechanical service cycles. The model development presented here is aimed at obtaining these data on a continuous scale, starting from failure initiation at the temperature exposed surface and up to the final failure of the TBCs in the form of complete delamination or spoliation. The expectation is that with the developed model and the data characterizing the complete process, one will be able to make a reasonable determination of the service life limitation of the TBCs. The model proposed here is based on consideration of a system of periodically spaced failure cells under thermal stress.

The developed numerical model takes advantage of the periodic nature of the problem. Thus, a free surface of the coating is represented as an array of dislocations in a manner similar to segments representing cracks. This technique turned out to be very effective and extremely reliable. Additionally, it bypasses an alternative path of solving the problem by using the Fourier Transform technique, and then dealing with numerical inversion of the results, a method used, for example, by Ballarini and Luo (1991).

2. The modeling concept

Shortly after the fabrication and placement in service of TBCs, a granular pattern of crack net formations on the surface is observed. Due to the high temperature gradients during the fabrication process, usually a net of surface cracks develops, which gives the appearance of a granular structure of the surface, often called a mud pie appearance. These surface cracks may be relatively short initially but, as is observed, they may reach the interface between the ceramic coating and the base metal in a relatively low number of service cycles. Typically, these cracks do not propagate through the interface into a substrate, but rather deflect and continue to grow along or near the interface. Thus, the main safe service period of TBCs is primarily dependent on the time, or number of service cycles, required for these cracks to cross the link holding the individual "grains" attached to the substrate. A two dimensional schematic illustration of this process is given in Fig. 1, which illustrates the model problem. The initial interface cracks are depicted as a periodically distributed net of cracks.

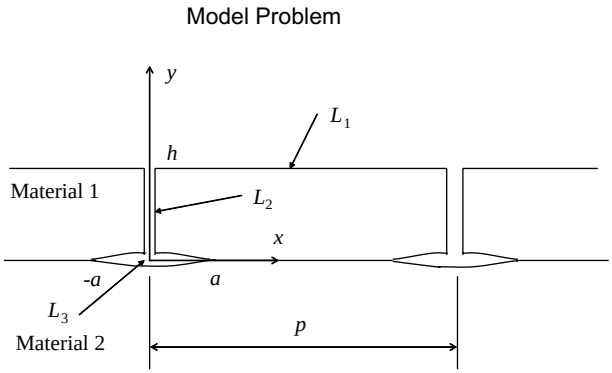

Fig. 1. Initiation and growth of interface cracks.

The modeling approach is based on the described observations. The practical goal is to determine the safe service time limit for the components equipped with TBCs. Taking a conservative approach, the aim of the modeling effort is determination of the time required for the cracks to bridge the interfacial link holding the coating layer. To achieve this, it is necessary to evaluate all crack growth driving parameters as they develop along the crack path. Determination of the stress intensity factors and the energy release rate as the crack progresses along the interface, is a necessary step toward service life prediction; this is the main scope of the present investigation. Here, we develop an analytical–computational relationship between these parameters and the thermo-mechanical loading parameters during the service cycle.

Although the process is three dimensional, a two dimensional problem could provide sufficient information regarding the nature of the process. The average "grain" size, that is, the parameter describing the initial spacing of the net of surface cracks, determines the size of periodic crack cells in a two-dimensional cross-section; that is period p, as illustrated in Fig. 1. The initial spacing of the surface cracks depends on the fabrication process parameters and, possibly, can be controlled by the manufacturing process.

Two alternative crack path directions are illustrated in Fig. 2. Development of the capability to identify a specific crack path option for a given TBS system is one of the goals of failure model development in this framework.

The developed model is based on the method of singular integral equations using appropriate periodic dislocation density functions as influence functions. The elastic fields are generated as a result of temperature or heat flux variation on the free surface of the ceramic coating. The essential steps of the development are described in the following sections, where more detailed attention is given to the development of

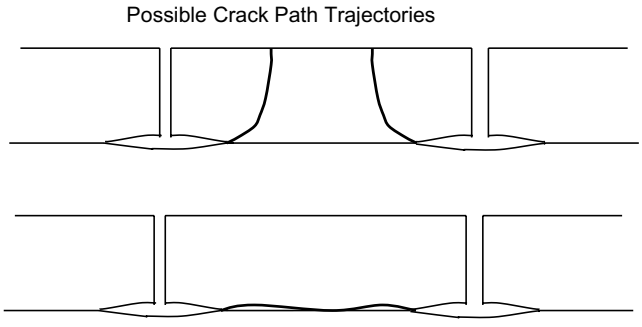

Fig. 2. Illustration of possible crack path trajectories.

the basic solution for the periodic array of dislocations interacting with the interface. This solution serves as an influence function for the system of singular integral equations and is given more attention because of the possible non-unique options of that solution. An important aspect of the presented solution is the loading due to the mismatch of the thermo-mechanical properties of the base and coating materials. The specific aspects typical for thin coatings are utilized in the analysis and discussed here. These aspects are also discussed in detail. In the follow up paper, the specifics of thick coatings will be addressed. Only the basic steps outlining the development of the integral equations and the numerical methods are presented here, because these techniques are well developed, although representing a free surface as a part of the system of singular integral equations seems to be a new step. The results illustrating the modeled case are based on the data for one of the typical TBC systems.

3. Dislocations and bimaterial interface

The stress potentials representing the interaction of a periodic set of dislocations with a biomaterial interface will be required for the analysis of the model problem. The derivation of these potentials is outlined using the general steps applicable to any singularities interacting with an interface separating two half spaces with different elastic properties. Although one may find a number of similar appearing derivations for a single dislocation or another singularity, typically, they are not general enough to be used for a periodic array of these defects. This is the reason for some details presented here.

The basic two dimensional elasticity relationships in terms of the complex potentials are, (1):

$$\begin{aligned}
&\sigma_{11}+\sigma_{22}=2(\phi'(z)+\overline{\phi'(z)}),\\
&\sigma_{22}-\sigma_{11}+2\mathrm{i}\sigma_{12}=2(\bar{z}\phi''(z)+\psi'(z)),\\
&u_1+\mathrm{i}u_2=\frac{1}{2\mu}\left[\kappa\phi(z)-z\overline{\phi'(z)}-\overline{\psi(z)}\right]_A^B,\\
&F_1+\mathrm{i}F_2=-\mathrm{i}\left[\phi(z)+z\overline{\phi'(z)}+\overline{\psi(z)}\right]_A^B.
\end{aligned}\tag{1}$$

Hear μ is the shear modulus, and $\kappa=3-4\nu$ in case of plane strain or $\kappa=(3-\nu)/(1+\nu)$ in case of plane stress consideration. ν is the Poisson ratio.

Placing the interface along the x-axis separating the upper and lower half planes of different elastic properties, use the following notations: for potentials ϕ_k, ψ_k with $k=1$ or 2, respectively for the upper and lower half planes, and use the same subscripts for the corresponding elastic constants. For the stresses, similarly use the superscript "+" and "−" when necessary.

Placing the dislocations (or other singularities) in the upper half plane, the solution there can be written as a superposition of singular functions, ϕ_0, ψ_0 and regular analytic functions ϕ_{10}, ψ_{10} in the upper half plane.

$$\phi_1(z)=\phi_0(z)+\phi_{10}(z),\quad \psi_1(z)=\psi_0(z)+\psi_{10}(z).\tag{2}$$

The solution in the lower half plane consists of regular analytic functions only. The equilibrium condition on the interface, $z=x$, in terms of these functions is:

$$\begin{aligned}
\sigma_{22}+\mathrm{i}\sigma_{12}&=\phi'_{10}(z)+\overline{\phi'_{10}(z)}+z\phi''_{10}(z)+\psi'_{10}(z)+\phi'_0(z)+\overline{\phi'_0(z)}+z\phi''_0(z)+\psi'_0(z)\\
&=\phi'_2(z)+\overline{\phi'_2(z)}+z\phi''_2(z)+\psi'_2(z).
\end{aligned}\tag{3}$$

The continuity of the displacement along the interface can be stated equivalently in terms of the continuity of the derivative of the displacement by x along the interface, $z=x$, or the conjugate of that derivative as done here, thus:

$$\frac{\partial}{\partial x}(u_1 - \mathrm{i}u_2) = \frac{1}{\mu_1}\left[\kappa_1\overline{\phi'_{10}(z)} - \phi'_{10}(z) - z\phi''_{10}(z) - \psi'_{10}(z) + \kappa_1\overline{\phi'_0(z)} - \phi'_0(z) - z\phi''_0(z) - \psi'_0(z)\right]$$
$$= \frac{1}{\mu_2}\left[\kappa_2\overline{\phi'_2(z)} - \phi'_2(z) - z\phi''_2(z) - \psi'_2(z)\right]. \tag{4}$$

Eqs. (3) and (4) are valid on the real axis. Each function in these equations represents the boundary value of a function analytic in the upper or the lower half plane. We rearrange these equations by placing all functions defining the boundary values of analytic functions in the upper half plane to the left in these equations, and the functions defining the boundary values of analytic functions in the lower half plane to the right. In doing so, one notes that the boundary value of a function analytic in a half plane specified along the real axis uniquely defines that function in the respective half plane, and the conjugate of the boundary value of that function defines an analytic function in the opposite half plane. *In both cases the functions defined by the boundary values on the real axis must vanish as z approaches infinity along the imaginary axis in the respective half plane*. After separating the functions in (3), (4) and applying the principle of analytical continuation to each side of these equations, one notes that on both sides of these equations, there must be functions analytic in the entire plane. The physical restrictions limit the values of the resulting functions at infinity to a constant. Therefore, as a result, one obtains four equations, the first two from Eq. (3), and the remaining two from Eq. (4). To simplify these equations the following notation is used with the corresponding values of the subscript:

$$P_k(z) = \phi'_k(z) + z\phi''_k(z) + \psi'_k(z). \tag{5}$$

Thus, the resulting equations are:

$$P_{10}(z) - \overline{\phi'_2}(z) + \overline{\phi'_0}(z) = C_1, \tag{6}$$

$$P_2(z) - \overline{\phi'_{10}}(z) - P_0(z) = C_1, \tag{7}$$

$$\frac{\kappa_1}{\mu_1}\overline{\phi'_0}(z) - \frac{1}{\mu_1}P_{10}(z) - \frac{\kappa_2}{\mu_2}\overline{\phi'_2}(z) = C_2, \tag{8}$$

$$-\frac{\kappa_1}{\mu_1}\overline{\phi'_{10}}(z) + \frac{1}{\mu_1}P_0(z) - \frac{1}{\mu_2}P_2(z) = C_2. \tag{9}$$

The standard notation, typically used in two-dimensional elasticity and adopted here, identifies analytic function $\overline{\phi'_k}(z)$ obtained by using the conjugate of the boundary value on x-axis of analytic function $\phi'_k(z)$. Both functions are analytic but in opposite half planes. Again, following the argument that the analytic functions formed from the boundary value on the real axis must vanish at infinity, the constants C_1 and C_2 must be set to zero and an additional restriction must be imposed:

$$\phi'_0(z), \quad P_0(z) \to 0, \quad \text{as } y \to -\infty. \tag{10}$$

Thus, solution of the system of equations (5)–(9) is:

$$P_{10}(z) = \frac{\kappa_1\mu_2 - \kappa_2\mu_1}{\mu_2 + \kappa_2\mu_1}\overline{\phi'_0}(z), \tag{11}$$

$$\phi'_{10}(z) = \frac{\mu_2 - \mu_1}{\mu_1 + \kappa_1\mu_2}\overline{P_0}(z), \tag{12}$$

$$P_2(z) = \frac{\mu_2(1+\kappa_1)}{\mu_1+\kappa_1\mu_2} P_0(z), \tag{13}$$

$$\phi_2'(z) = \frac{\mu_2(1+\kappa_1)}{\mu_2+\kappa_2\mu_1} \phi_0'(z). \tag{14}$$

3.1. Single dislocation in the upper half plane

To obtain a complete solution for the case of a single dislocation, use the stress potentials for a single dislocation at $z = t$, Im $t > 0$, in an infinite plane as the singular functions in Eqs. (11)–(14); thus:

$$\phi_0'(z) = \frac{\mu_1}{\pi i(1+\kappa_1)} \cdot \frac{b}{z-t}, \quad \psi_0'(z) = -\frac{\mu_1}{\pi i(1+\kappa_1)} \cdot \frac{\bar{b}}{z-t} - \bar{t}\phi_0''(z), \tag{15}$$

$$P_0(z) = \frac{\mu_1}{\pi i(1+\kappa_1)} \cdot \frac{b-\bar{b}}{z-t} + (z-\bar{t})\phi_0''(z). \tag{16}$$

The restriction (10) is satisfied and, therefore, Eqs. (2), (5), (11)–(16) complete the solution. To obtain the solution for a dislocation positioned in the lower half plane, Im $t < 0$, one needs simply to rotate the subscripts 1 and 2 in Eqs. (11)–(16).

3.2. Single dislocation on the interface

A special case of a dislocation positioned on the interface can be obtained as a limit case when Im $t \to 0$. Thus, noting that $\bar{t} = t$ in (15), (16) and using Eqs. (2), (11)–(14), the result is:

$$\phi_j'(z) = \frac{\mu_1\mu_2}{\pi i(\mu_j+\kappa_j\mu_k)} \cdot \frac{b}{z-t}, \quad P_j(z) = -\frac{\mu_1\mu_2}{\pi i(\mu_k+\kappa_k\mu_j)} \cdot \frac{\bar{b}}{z-t}. \tag{17}$$

In (17) the subscripts $j = 1$, $k = 2$ for the upper half plane and $j = 2$, $k = 1$ for the lower half plane. The validity of the solution as a limit of the solution in the upper or lower half plane may be questioned due to the singularity on the boundary which was used earlier for the analytical continuation. To prove that the functions (17) actually represent the solution, one must calculate the total displacement gain over a closed contour surrounding point t. The resulting displacement should equal b. Additionally, the net force calculated over a closed contour surrounding t must be zero. On the path of the contour through the upper half plane functions (17) should be used with $j = 1$, $k = 2$ and on the remainder path $j = 2$, $k = 1$. These calculations were carried out using a circular path and the solution (17) was proven to be correct.

3.3. Periodic distribution of dislocations along a line parallel to the interface in the upper half plane

To obtain a solution for periodically distributed dislocations, one needs only to replace the singular terms in (15)–(17) by a periodic function which is in effect a superposition of the periodic distribution of these terms. Eqs. (11)–(14) remain in effect after replacing functions with subscript 0 by the functions with subscript $p0$ given below. In addition a constant could always be added to these functions. This addition is necessary to enforce the condition (10). Thus, the result for the distribution with period p in the upper half plane, Im $t > 0$, is:

$$\phi_{p0}'(z) = \frac{\mu_1}{(1+\kappa_1)} \cdot \frac{b}{pi} \left(\cot\frac{\pi}{p}(z-t) - i \right), \tag{18}$$

$$\psi'_{p0}(z) = -\frac{\mu_1}{(1+\kappa_1)} \cdot \frac{\bar{b}}{p\mathrm{i}} \left(\cot \frac{\pi}{p}(z-t) - \mathrm{i} \right) - \phi'_{p0}(z) - (z-t+\bar{t})\phi''_{p0}(z), \tag{19}$$

$$P_{p0}(z) = \frac{\mu_1}{(1+\kappa_1)} \cdot \frac{-\bar{b}}{p\mathrm{i}} \left(\cot \frac{\pi}{p}(z-t) - \mathrm{i} \right) + (t-\bar{t})\phi''_{p0}(z). \tag{20}$$

Functions (18)–(20) do not vanish as $y \to +\infty$. They correspond to a remote normal stress parallel to the interface and a rotation, Ω:

$$\sigma_{11}^{+\infty} = -\frac{8b_1}{p} \cdot \frac{\mu_1}{1+\kappa_1}, \quad \Omega^{+\infty} = -\frac{b_2}{p}. \tag{21}$$

The presence of this remote stress and rotation on one side of the interface is physically acceptable, and this special feature of the interface problems will be discussed in greater detail below. To eliminate the presence of these constants *the condition of zero of the total cumulative dislocation net over the period must be used in the formulation of the problem.*

To obtain the stress functions for *a periodic dislocation array positioned in the lower half plane*, Im $t < 0$, in addition to rotating the subscripts 1 and 2 in Eqs. (11), (12), (13), (14) and (18), (19), (20), a negative sign in front of the constant i must be changed to positive, to enforce condition (10) which now should be satisfied as $y \to +\infty$.

3.4. Periodic distribution of dislocations on the interface

Again, using subscripts $j = 1$, $k = 2$ for the upper half plane and $j = 2$, $k = 1$ for the lower half plane, the stress functions are:

$$\begin{aligned} \phi'_j(z) &= \frac{\mu_1\mu_2}{(\mu_j + \kappa_j\mu_k)} \cdot \frac{b}{p\mathrm{i}} \left(\cot \frac{\pi}{p}(z-t) - \mathrm{i} \right), \\ P_j(z) &= -\frac{\mu_1\mu_2}{(\mu_k + \kappa_k\mu_j)} \cdot \frac{\bar{b}}{p\mathrm{i}} \left(\cot \frac{\pi}{p}(z-t) - \mathrm{i} \right). \end{aligned} \tag{22}$$

Solution (22) is formed to enforce condition (10) for the lower half plane. A second version of this solution can be formed with stress functions vanishing in the upper half plane.

4. The stress discontinuity at the interface

A stress state along the interface inevitably includes a discontinuity of a normal stress component parallel to the interface. General relationships between the stress components and rotation discontinuities are obtained using relationships (3) and (4) without singular terms:

$$\frac{1+\kappa_1}{\mu_1}\sigma_{11}^{+} = \frac{1+\kappa_2}{\mu_2}\sigma_{11}^{-} + \frac{3(\mu_2-\mu_1) + \kappa_2\mu_1 - \kappa_1\mu_2}{\mu_1\mu_2}\sigma_{22}, \tag{23}$$

$$\frac{1+\kappa_1}{\mu_1}\theta^{+} = \frac{1+\kappa_2}{\mu_2}\theta^{-} + \frac{\mu_1-\mu_2}{\mu_1\mu_2}\sigma_{12}. \tag{24}$$

This mandatory presence of the discontinuous stress component creates several options for problems involving an interface. For example, it is always possible to create a situation when on one side of the interface this stress component is zero. Naturally, any prediction of crack propagation in the vicinity of the interface under these conditions will be significantly different from the case when a normal stress parallel

to the interface is set to be zero on the opposite side of the interface. Therefore, any problem in an infinite plane with an interface and stresses vanishing at infinity on both sides cannot truly represent a practical case where at least on one side these stresses must be present.

A periodic problem by its nature cannot have well defined stress values at infinity along the direction defining the period of the problem. In the considered case, the stress values in the vicinity of the interface along the x-axis vary within the interval defined by the period of the problem. However, one can discuss the net stress over the period or, equivalently, an average stress within the period. The average normal stress below the interface created by periodically distributed dislocations positioned in the upper half plane is:

$$\sigma_{11}^{-} = \frac{1}{p}\mathrm{Re}\left[3\phi_2 - \int P_2\,\mathrm{d}x + 2\mathrm{i}y\phi_2'\right]_{x=0}^{x=p}$$
$$= \frac{2\mu_1\mu_2}{p^2}\left[\frac{y}{\mu_2+\kappa_2\mu_1} + \frac{\mathrm{Im}(t)}{\mu_1+\kappa_1\mu_2}\right]\mathrm{Re}\left[b\cot\frac{\pi}{p}(z-t)\right]_{x=0}^{x=p} = 0. \tag{25}$$

Following Eq. (23), the average stress above the interface is zero as well. That, of course, does not exclude stress discontinuity at any point along the interface.

Thus, the only non zero average normal stress component parallel to the interface under the given conditions could be generated by the temperature field. There are three possibilities for the stress state of the considered system of finite thickness elastic layer on a semi-infinite elastic plane with different elastic and thermal properties: (a) both the coating and the plane are completely restrained in the direction parallel to the interface, so no displacement mismatch can develop and the stress differences are only due to the temperature fields; (b) both the coating and the plane are free to expand in the direction parallel to the interface and the stress state on both sides should compensate for mismatch of the thermo-mechanical properties and the temperature distribution; (c) a partial constraint is applied for the thermal expansion on one side or uneven constraint on both sides. Case (a) at best represents a very special situation and is not very practical, since it generates only compressive stresses, although it was considered by Rizk and Erdogan (1989). Case (c) cannot be applied to a semi-infinite plane, and it represents special situations which cannot be generalized. Case (b) describes most appropriately the situation applicable to thin TBCs. The base material represented as a semi-infinite plane must be allowed to expand freely as would, generally speaking, a working component. A thin protective layer cannot constrain the thermal expansion of a much thicker base material. A simple energy consideration supports this conclusion. Considering a single periodic segment, one notes that *to constrain thermal expansion of a semi-infinite elastic strip, the coating would have to concentrate an infinite amount of the strain energy per unit length*. This is a physically unacceptable situation, and, therefore, the condition of free thermal expansion of the base material must be employed.

The only stress component generated by the temperature field within the considered plane is a normal stress parallel to the interface, σ_{11}. With the condition of zero thermal stress in the direction perpendicular to the interface, this stress is determined as

$$\sigma_{11} = \frac{8\mu}{1+\kappa}\varepsilon_{11} - \frac{8\mu}{1+\kappa}\alpha_{\mathrm{t}}T, \tag{26}$$

for the plane stress case and in case of plane strain the last term must be multiplied by $(1+\nu)$. T in (26) is the temperature increase from the neutral, stress free temperature state, and α_t is the coefficient of linear thermal expansion. The same argument that we used to justify the free expansion of the base material in the x direction on the plane could be used in the perpendicular direction along the interface. Therefore, using the plane stress condition for the thermal stress determination seems to be a reasonable choice. By allowing the base material the free expansion, the coating layer will experience additional stress

$$\sigma_{11}^{+} = \frac{8\mu^{+}}{1+\kappa^{+}}\alpha_{\mathrm{t}}^{-}T_{\mathrm{i}}, \tag{27}$$

where T_i is the interface temperature increase from the neutral, stress free temperature state. For the problem in an infinite domain this stress (27) in a thin coating layer should be applied uniformly across the thickness of the coating. The elastic constants in (27) correspond to the material of the coating, and the coefficient of thermal expansion corresponds to the base material in the lower half plane. Thus the total stress in the coating is a superposition of stresses (27) and (26):

$$\sigma_{11}^{+} = \frac{8\mu^{+}}{1+\kappa^{+}}\varepsilon_{11}^{+} - \frac{8\mu^{+}}{1+\kappa^{+}}\alpha_{t}^{+}T + \frac{8\mu^{+}}{1+\kappa^{+}}\alpha_{t}^{-}T_{i}. \tag{28}$$

The temperature distribution is determined by solving the thermal conductivity problem with the boundary conditions relevant to the TBCs service conditions.

5. Temperature distribution

The temperature field considered in this case is due to the changes in the applied temperature at the free surface of the protective coating. Temperature changes due to elastic deformation are neglected. Thus, a decoupled system of governing equations is used. The solutions of the thermal conductivity equation with the boundary conditions at the free surface and the interface determine the temperature field. A heat conduction problem which involves cracks directed transversely to the potential heat flux generally needs to include additional conditions at the crack surfaces. These conditions and their limitations will be discussed in our follow up paper dealing with thick coatings. In the considered case of thin coatings with implication of a free thermal expansion of the base material, the effect of the heat flux change due to the presence of interface cracks on the resulting stress field is not anticipated to be significant. Therefore, a one dimensional heat conduction problem can be considered. The governing equation is

$$\frac{\partial T_j}{\partial t} = \beta_j \frac{\partial^2 T_j}{\partial y^2} \tag{29}$$

with $j = 1$ for the region occupied by the coating, $0 < y < h$, and $j = 2$ for the base material, $y < 0$. β_j in (29) is the thermal diffusivity coefficient for the corresponding region identified by subscript j.

There are two typical boundary conditions at the free surface of the coating when the temperature is prescribed, Problem 1, and when the heat flux is prescribed, Problem 2, at the surface $y = h$. Thus, for Problem 1 we use

$$T_1(h,t) = T_S, \quad \text{for } t > 0, \tag{30}$$

and for Problem 2,

$$k_1 \frac{\partial T_1(h,t)}{\partial y} = -q_S, \quad \text{for } t > 0, \tag{31}$$

where q_S is the heat flux at the surface.

In both Problems, the boundary conditions at the interface state the continuity of the temperature and the heat flux

$$T_1(0,t) = T_2(0,t) \quad \text{and} \quad k_1 \frac{\partial T_1(0,t)}{\partial y} = k_2 \frac{\partial T_2(0,t)}{\partial y}, \tag{32}$$

where k_j is the thermal conductivity for the corresponding region. The temperature at the point infinitely remote from the interface remains constant and is equal to the initial temperature of the system,

$$T_1(y,0) = T_2(y,0) = T(-\infty,t) = T_0. \tag{33}$$

The solutions for both problems are obtained by using the Laplace transformation method. The solutions are:

Problem 1:

$$T_1(y,t) = (T_S - T_0)\left\{\sum_{n=0}^{\infty}(-1)^n \Lambda^{n+1}\operatorname{erfc}\left[\frac{(2n+1)h+y}{2\sqrt{\beta_1 t}}\right] + \sum_{n=0}^{\infty}(-1)^n \Lambda^n \operatorname{erfc}\left[\frac{(2n+1)h-y}{2\sqrt{\beta_1 t}}\right]\right\} + T_0$$

$$= (T_S - T_0)\left\{\operatorname{erfc}\left[\frac{h-y}{2\sqrt{\beta_1 t}}\right] + \sum_{n=1}^{\infty}(-1)^n \Lambda^n \left[\operatorname{erfc}\left[\frac{(2n+1)h-y}{2\sqrt{\beta_1 t}}\right] - \operatorname{erfc}\left[\frac{(2n-1)h+y}{2\sqrt{\beta_1 t}}\right]\right]\right\} + T_0$$

$$0 \leqslant y \leqslant h, \tag{34}$$

$$T_2(y,t) = (T_S - T_0)\left\{(1+\Lambda)\sum_{n=0}^{\infty}(-1)^n \Lambda^n \operatorname{erfc}\left[\frac{(2n+1)h-\eta y}{2\sqrt{\beta_1 t}}\right]\right\} + T_0, \quad y \leqslant 0 \tag{35}$$

with $\Lambda = \dfrac{1-\eta\frac{k_2}{k_1}}{1+\eta\frac{k_2}{k_1}}$ and $\eta = \sqrt{\dfrac{\beta_1}{\beta_2}}$.

Problem 2:

$$T_1(y,t) = -\frac{q_S}{k_1}\sum_{n=0}^{\infty}\Lambda^{n+1}\left(2\sqrt{\frac{\beta_1 t}{\pi}}\exp\left(-\frac{[(2n+1)h+y]^2}{4\beta_1 t}\right) - [(2n+1)h+y]\operatorname{erfc}\left(\frac{(2n+1)h+y}{2\sqrt{\beta_1 t}}\right)\right)$$

$$-\frac{q_S}{k_1}\sum_{n=0}^{\infty}\Lambda^{n}\left(2\sqrt{\frac{\beta_1 t}{\pi}}\exp\left(-\frac{[(2n+1)h-y]^2}{4\beta_1 t}\right) - [(2n+1)h-y]\operatorname{erfc}\left(\frac{(2n+1)h-y}{2\sqrt{\beta_1 t}}\right)\right) + T_0$$

$$0 \leqslant y \leqslant h, \tag{36}$$

$$T_2(y,t) = -(1+\Lambda)\frac{q_S}{k_1}\sum_{n=0}^{\infty}\Lambda^n\left(2\sqrt{\frac{\beta_1 t}{\pi}}\exp\left(-\frac{[(2n+1)h-\eta y]^2}{4\beta_1 t}\right)\right.$$

$$\left.-[(2n+1)h-\eta y]\operatorname{erfc}\left(\frac{(2n+1)h-\eta y}{2\sqrt{\beta_1 t}}\right)\right) + T_0, \quad y \leqslant 0. \tag{37}$$

The solution for the temperature in the layer of the first problem is given in two forms for easy verification by inspection. Both solutions can be easily verified and, therefore, the details are omitted.

6. The integral equations

The complete solution for the problem is set in the form of a superposition of three arrays of dislocations on the intervals identified in Fig. 1, as L_1, L_2, and L_3. Thus, the stress functions are represented as integrals (38), (39).

$$\phi_1'(z,t) = \int_{L_1}\phi_{11}'(z,t,b_1(v))\,\mathrm{d}v + \int_{L_2}\phi_{11}'(z,t,b_2(v))\,\mathrm{d}v + \int_{L_3}\phi_{12}'(z,t,b_3(v))\,\mathrm{d}v, \tag{38}$$

$$\psi_1'(z,t) = \int_{L_1}\psi_{11}'(z,t,b_1(v))\,\mathrm{d}v + \int_{L_2}\psi_{11}'(z,t,b_2(v))\,\mathrm{d}v + \int_{L_3}\psi_{12}'(z,t,b_3(v))\,\mathrm{d}v. \tag{39}$$

In Eqs. (38) and (39) functions with subscript 11 represent complete solutions for a periodic set of dislocations in the upper half plane, and functions with subscript 12 represent solutions for a periodic set of dislocations distributed along the interface. The unknown dislocation densities $b_1(v)$, $b_2(v)$, and $b_3(v)$ are found as the solution of the system of singular integral equations of Cauchy type. The integral equations are derived as statements of traction free conditions on the corresponding intervals representing a free surface and the cracked regions (40).

$$\begin{aligned} &\text{on } L_1 : y = \mathrm{i}h, \quad 0 < x < p \Rightarrow \sigma_{22} + \mathrm{i}\sigma_{12} = 0, \\ &\text{on } L_2 : x = 0, \quad 0 < y < h \Rightarrow \sigma_{11} + \mathrm{i}\sigma_{12} + \sigma_{11}^{+} = 0, \\ &\text{on } L_3 : y = 0, \quad -a < x < a \Rightarrow \sigma_{22} + \mathrm{i}\sigma_{12} = 0. \end{aligned} \tag{40}$$

The loading stress in the second equation in set (40) represents the thermal stress which is defined by Eq. (28). The configuration depicted in Fig. 1. represents the main problem of the considered set. Additional problems represent gradual failure development beginning with the surface crack development along interval L_2, call it Case 1. The crack growth along L_2 is followed until the crack reaches the interface or branches out before the interface is reached, Case 2, and Case 3 represents crack branching along the interface as identified in set (40). In Case 2, interval L_3 has $y > 0$.

The resulting system of integral equations, as is typical for these type of problems, must have an additional set of supplemental conditions. These conditions are usually dictated by the physical restrictions on the solutions. The unknown dislocation densities on the corresponding intervals determine the singularity of the stress field in the vicinity of the crack tips or the corners of the elastic region surrounded by the described integrals. There is one supplementary condition for each integral equation. On the free surface the condition of the zero net dislocation density is stated,

$$\int_{L_1} b_1(v)\,\mathrm{d}v = 0. \tag{41}$$

Condition (41) is necessary to cancel the remote stress and rotation generated by the periodically distributed dislocation set, Eq. (21). Because of the periodic nature of the problem the solution with condition (41) always produces dislocation density with zero values at the ends of the interval L_1. The physical condition to be enforced for the developing surface crack along interval L_2 is the condition of bounded stress field in the vicinity of the corner formed by the crack and the free surface, that is

$$b_2(z = 0 + \mathrm{i}h) = 0. \tag{42}$$

As the surface crack develops within the protective layer the singularity of the dislocation density at the crack tip must be proportional to the square root, and when the crack reaches the interface, the singularity order, λ, changes and is determined by the equation

$$2\lambda^2(A_d - B_d)(1 + B_d) - A_d + B_d^2 + (1 + B_d)(1 - B_d)\cos(\lambda\pi) = 0, \tag{43}$$

where the following notations are used (Dundur's parameters)

$$\begin{aligned} A_d &= \frac{\mu_2(\kappa_1 + 1) - \mu_1(\kappa_2 + 1)}{\mu_2(\kappa_1 + 1) + \mu_1(\kappa_2 + 1)}, \\ B_d &= \frac{\mu_2(\kappa_1 - 1) - \mu_1(\kappa_2 - 1)}{\mu_2(\kappa_1 + 1) + \mu_1(\kappa_2 + 1)}. \end{aligned} \tag{44}$$

The singularity of the dislocation density is enforced by the numerical scheme used to solve the system of integral equations. At the point when the crack on L_2 branches into segments parallel, $y_3 > 0$, or along the interface, $y_3 = 0$, an additional physical condition is enforced. That is the condition of bounded stress field in the vicinity of the new corner formed by the crack on L_2 and a new crack branch,

$$b_2(z = 0 + iy_3) = 0. \tag{45}$$

The singularity of the dislocation density at the crack tips of the branched segments is the square root if the branch is above the interface, and it is

$$b_3(v) \sim (v - a)^{\alpha}(b - v)^{\beta}, \tag{46}$$

where a and b represent left and right crack tips, respectively and

$$\begin{aligned} \alpha &= -0.5 - i\varepsilon, \\ \beta &= -0.5 + i\varepsilon \end{aligned} \tag{47}$$

with

$$\varepsilon = \frac{1}{2\pi} \ln \frac{1 - B_d}{1 + B_d}. \tag{48}$$

The numerical scheme of the solution is based on Gauss-Chebyshev quadrature when only square root singularities are involved, and on Gauss-Jacobean quadrature which is based on Jacobean polynomials on the segments with other singularity types. The general arrangement of the numerical scheme follows the scheme described by Rubinstein (1986) and Rubinstein and Choi (1988).

7. Numerical examples and discussion

The numerical examples were computed using the data used in experiments described by Zhu et al. (1998). The material properties are summarized in Table 1. The definitions of the stress intensity factors and the energy release rate along the interface used in the computations are consistent with the definitions introduced by Rice and Sih (1965). Thus, the complex valued stress intensity factors are

$$\begin{aligned} K(b) &= \sqrt{2\pi} \lim_{z \to b} (z - b)^{-\beta} [\sigma_{22}(z) + i\sigma_{12}(z)], \\ K(a) &= \sqrt{2\pi} \lim_{z \to a} (a - z)^{-\alpha} [\sigma_{22}(z) + i\sigma_{12}(z)] \end{aligned} \tag{49}$$

and the energy release rate, G, is

$$G = \frac{1}{16} \left(\frac{1 + \kappa_1}{\mu_1} + \frac{1 + \kappa_2}{\mu_2} \right) (K_1^2 + K_2^2). \tag{50}$$

The physical parameters are presented as dimensionless values by using the following definitions

Table 1
Physical and mechanical properties of thermal barrier coating system used in calculation (Zhu et al., 1998)

Materials properties	Plasma sprayed ZrO_2–8 wt%Y_2O_3	4120 steel
Young's modulus, E (GPa)	70.0	180.0
Poisson ratio, υ	0.25	0.25
Heat capacity, c (J/kg °K)	582	456.4
Thermal conductivity, k (W/m °K)	0.9	46.7
Thermal expansion coefficient, α_t (10^{-6}/°K)	10.8	14.2
Density, ρ (kg/m^3)	5236	7850
Thermal diffusivity, β (10^{-7} m^2/s)	2.953	130.3
Shear modulus, μ (GPa)	28.0	72.0

$$K_0 = \frac{K}{\sigma_0\sqrt{\pi h}}, \quad G_0 = \frac{G}{\frac{1}{8}\sigma_0^2\pi h\frac{1+\kappa_1}{\mu_1}}, \quad \text{with } \sigma_0 = -\frac{E_1\alpha_1\Delta T_S}{1-\nu_1} \text{ or } \sigma_0 = \frac{E_1}{1-\nu_1}\alpha_1\frac{q}{k_1}h, \tag{51}$$

where K is the stress intensity factor, G is the energy release rate, E is Young's modulus, μ is shear modulus, α_t is thermal expansion coefficient, ΔT_s is the temperature increase at the surface (Problem 1), q is surface heat flux (Problem 2) k is thermal conductivity, and h is the thickness of the thermal barrier coating. The stress in the presented data is normalized by σ_0 given in (51).

The service conditions of TBCs typically involve complicated loading patterns which may be based on variation of surface temperature or surface heat flux. The loading patterns could be in a form of step loading, as in the case of constant temperature environment or an exposure to a constant thermal flux, or as a cyclic variation of these conditions. The developed solution is capable of handling any of these possibilities and their combinations. However, to capture the main physical aspect of potential failure development in TBCs, a limited number of basic examples are presented. The results are arranged in the order of potential failure development starting with cracks leading from the free surface to the interface.

As was discussed earlier, there are two loading components on the developing cracks in thin protective coatings. One loading component is proportional to the local temperature increase at each specific location, and another is the loading stress developed in the direction parallel to the interface due to the mismatch of thermo-mechanical parameters of the materials separated by the interface. In the case of the considered material system, initially the thermal stress within the coating is negative, but as the temperature flux reaches the interface, the interface temperature increases, initiating expansion of the base material, and the loading stress becomes positive, gradually increasing and becoming a dominant loading component. In Fig. 3, the development of stress components acting parallel to the interface at three different locations are presented. The chosen locations to illustrate the effect are at the free surface, in the middle of the coating layer, and on the coating side at the interface. The data in Fig. 3a was generated under the condition of step loading of constant temperature at the surface, up to 850 °C, and in Fig. 3b the condition of step loading by the applied surface heat flux of value of is 5×10^5 W/m^2 was used. These values were taken from the experiments published by Zhu et al. (1998).

The development of a system of periodically spaced cracks leading through the coating from the free surface toward the interface is typically observed shortly after components with TBC protection are placed in service. These cracks are often explained by the presence of residual stresses from the processing of TBCs. The data plotted in Fig. 4 demonstrates that this does not have to be the case. There is sufficient driving force acting on these cracks due to the thermal stresses developed in the coating layer during service,

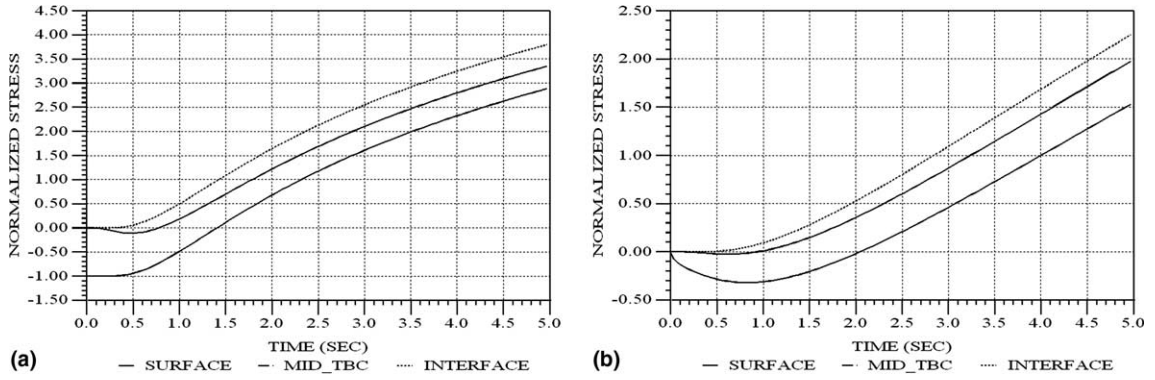

Fig. 3. The normal stress component parallel to the interface versus time. (a) constant temperature is maintained at the surface, (b) constant flux is maintained at the surface.

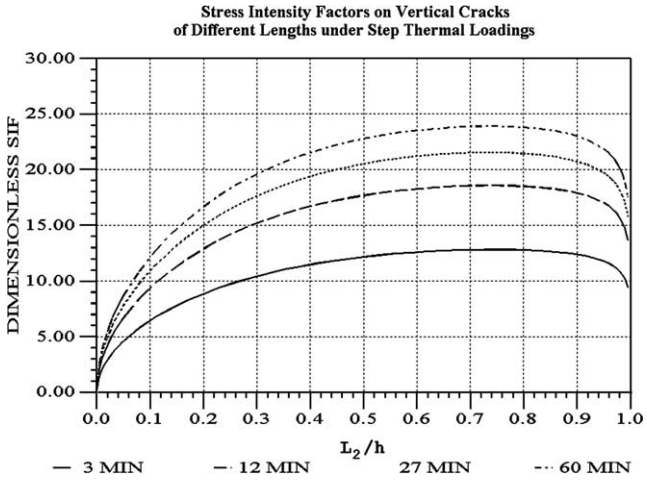

Fig. 4. Stress intensity factors at the crack growing from the free surface toward the interface.

as demonstrated by the aggressive growth of the stress intensity factor acting on these cracks as they develop. It is natural that the driving stress intensity factor drops as these cracks approach the interface. This is due to the anticipated change in singularity which for the chosen material combination is weaker than the square root, and an additional factor is the free expansion of the base material typical for thin TBCs. The combination of these factors promotes crack branching in a direction parallel to the interface.

In Fig. 5, an analysis of the stress intensity factors driving the branched crack segments parallel to the interface and located above the interface is presented. The developed high values of positive Mode II stress intensity factors suggest that the direction of growth of these cracks during the initial state will be deflected toward the interface. Crack branching and growth along the interface appears to be more stable, Fig. 6. The data in Figs. 4–6 were developed using TBC thickness $h = 1.5$ mm, crack period $p = 5$ mm, and the surface temperature 850 °C. The crack growth was assumed to take place at a specific time as indicated in the figures. There is a possibility of some variation of the presented data under different sets of parameters. How-

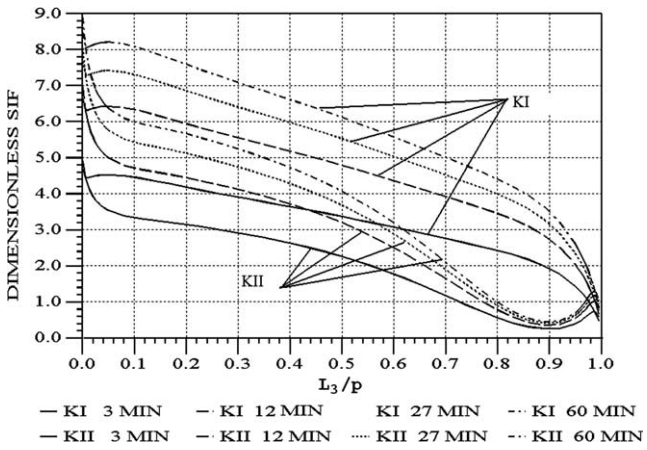

Fig. 5. Stress intensity factors acting on a crack branched above the interface, parallel to the interface, $L_2 = 0.75h$.

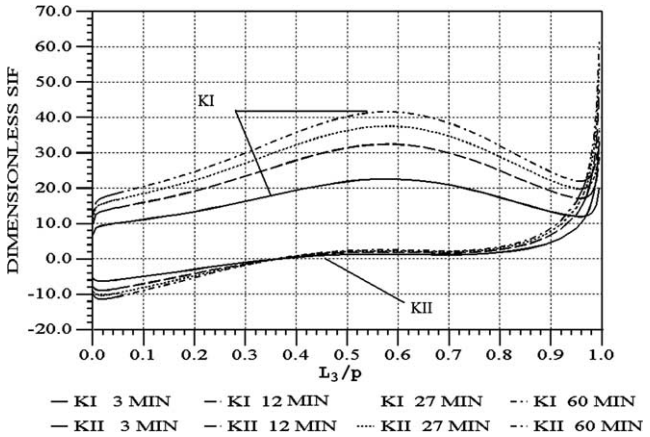

Fig. 6. Dimensionless stress intensity factors acting on the interface cracks under constant temperature conditions at the coating surface.

ever, the consistency of the developed patterns suggests the accuracy of the qualitative character of the developing process.

The pattern of development of the driving stress intensity factor as the crack grows along the interface indicates that this path is the preferable one. This preference for crack path development takes place until the crack tip reaches the critical point when crack growth resistance develops. This development takes place as the magnitude of the Mode I stress intensity factor drops without a change in the applied load. A segment of the crack path with the developed crack growth resistance is clearly shown for the branched cracks propagating along the interface, Fig. 6. As the interface cracks are closing the gap within the periodic cells, crack growth resistance drops and conditions favoring spontaneous failure of the TBC take place. The conditions for possible crack path deflection toward the free surface do not develop in the considered case, but this possibility exists for different geometrical combinations after the crack tip passes the critical point. Locations of the critical points and the patterns of the crack growth resistance depend on geometrical combinations and the time of crack growth. However, the presence of these characteristics explains the service time difference between development of the cracks leading toward the interface and the relatively slow time of crack growth along the interface.

A few sets of numerical examples were generated to represent the stress states developed under various loading conditions, such as a thermal load applied as constant temperature at the surface; a cyclic temperature load at the surface; constant thermal flux at the surface; and a cyclic thermal flux at the surface. The analysis of the case of a constant surface temperature plays a guiding role in understanding the cyclic temperature case and evolution of the residual stresses generated by the fabrication process. The case of the step function loading at the surface, of course, serves as the base for development of any other solution with a more complex loading pattern. Examples of the variation of the energy release rate at branched cracks along the interface under a cyclic temperature variation at the surface are shown in Fig. 7. The crack positions in Fig. 7 are considered as stationary to illustrate the effect of the loading cycle. An important characteristic to be noted here is the continuous increase of the energy release rate amplitude due to the time delay in local temperature variation and the change in the variation pattern due to the nature of the heat conduction process. These effects become more significant with increased exposure to cyclic thermal loading. There is a noticeable cumulative effect on the crack growth potential due to the cyclic loading at each crack tip position. This is a detrimental factor for the service life prediction tools development.

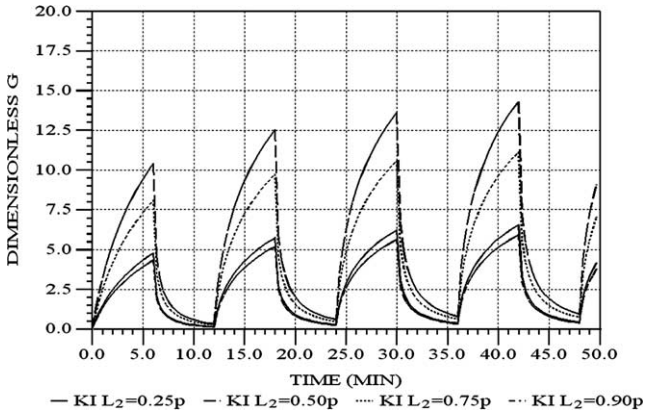

Fig. 7. Dimensionless energy release rate development on the interface cracks under cyclic temperature variation at the surface.

The analysis of cases involving heat flux prescribed at the surface show similar patterns of behavior of all major parameters. However, one must note that the heat flux condition at the surface, if not coupled with the temperature of the surrounding environment, leads to an unreasonable increase of the surface temperature. The coupling with the surrounding environment adds radiation or convection conditions which offset the otherwise continuous temperature increase. These additional conditions involve an additional set of variables, which at this time, as we concentrate on the basic aspects of the process, were not introduced. However, the developed solution is capable of including any possible combination of these conditions into consideration.

8. Conclusions

A comprehensive analytical–computational model simulating failure progression in thin thermal barrier coatings has been developed. The model is based on a periodically spaced system of failure sites. The computational model is capable of following a system of surface cracks as they initiate at the surface exposed to high temperature, develop while crossing the coating layer, and eventually branch off along the coating-base material interface. As is commonly observed, the simulations demonstrate that the crack branching along the interface is the most stable crack path development under the described conditions. The numerical simulations of practical cases explain the experimentally observed patterns of failure and the failure development time relationships between the different segments of the crack growth within the TBCs. While, as noted, stable crack growth can occur primarily along the interface, of particular significance is the development of crack growth resistance during a portion of crack growth along the interface. An accurate prediction of the crack growing segment length and the time it takes to develop under the presence of crack growth resistance, could be the key to safe service life prediction of the components with TBCs.

The developed results are based on a material system which, as it seems from the elastic stiffness of these materials, would prevent crack propagation across the interface. However, as was shown, the same effect will take place in any material combination under the described thermal loading. Thus, the interface toughness and fracture resistance development along the interface are the only factors determining the durability of the TBCs.

The presented results were developed by considering a periodic system and could not be foreseen from consideration of a single T-shaped crack.

The developed data helps to understand the interface crack driving force evolution as cracks are developing under thermal loadings in TBCs. The present work is a basic development toward a service life prediction system development for TBCs, and the data developed here could be used as guiding information for TBC design.

The developed computational model takes advantage of the considered periodic system and is based on a direct solution, bypassing methods based on integral transformation. Although the aim of the presented analysis was thermal loading, the developed method can be used for failure modeling under general loadings.

Acknowledgment

The work presented here was supported by NASA under Grant NAG3-2689 and in part by Grant NCC3-946.

References

Ballarini, R., Luo, H., 1991. Green's functions for dislocations in bonded strips and related crack problems. International Journal of Fracture 50, 239–262.

Evans, A.G., He, M.Y., Hutchinson, J.W., 2001. Mechanics-based scaling laws for the durability of thermal barrier coatings. Progress in Materials science 46, 249–271.

Hsueh, C.H., 2002. Thermal stresses in elastic multilayer system. Thin Solid Films 418, 182–188.

Hutchinson, J.W., Suo, Z., 1992. Mixed mode cracking in layered materials. Advances in Applied Mechanics 29, 63–191.

Hutchinson, J.W., Lu, T.J., 1995. Laminate delamination due to thermal gradients. Journal of Engineering Materials and Technology 117, 386–390.

Lee, Y., Erdogan, F., 1998. Interface cracking of FGM coatings under steady state heat flow. Engineering Fracture Mechanics 59 (3), 361–380.

Qian, G., Nakamura, T., Berndt, C.C., 1998. Effects of thermal gradient and residual stress on thermal barrier coating fracture. Mechanics of Materials 27, 91–110.

Rice, J.R., Sih, G.C., 1965. Plane problems of cracks in dissimilar media. Journal of Applied Mechanics 32, 418–423.

Rizk, A.A., Erdogan, F., 1989. Cracking of coated materials under transient thermal stresses. Journal of Thermal Stresses 12, 125–168.

Rubinstein, A.A., 1986. Macrocrack–microdefect interaction. Journal of Applied Mechanics. Transactions of the ASME 53, 505–510.

Rubinstein, A.A., Choi, H.C., 1988. Macrocrack interaction with a transverse array of parallel microcracks. International Journal of Fracture 36, 15–26.

Shulze, G.W., Erdogan, F., 1998. Periodic cracking of elastic coatings. International Journal of Solids and Structures 35, 3615–3634.

Zhu, D., Miller, R.A., 1997. Determination of creep behavior of thermal barrier coatings under laser imposed temperature and stress gradients. NASA Technical Memorandum 113169.

Zhu, D., Miller, R.A., 1998a. Influence of high cycle thermal loads on thermal fatigue behavior of thick thermal barrier coatings. NASA technical report, 3–10, NASA TP-3676.

Zhu, D., Miller, R.A., 1998b. Investigation of thermal high cycle and low cycle fatigue mechanisms of thick thermal barrier coatings. NASA/TM-1998-206633.

Zhu, D., Miller, R.A., 1998c. Investigation of thermal high cycle and lower fatigue mechanism of thick thermal barrier coatings. Materials Science and Engineering A245, 212–223.

Zhu, D., Ghosn, L.J., Miller, R.A., 1998. Effect of layer-graded bond coats on edge stress concentrations and oxidation behavior of thermal barrier coatings. NASA/TM-1998-208505.